JOURNAL OF SOLID STATE CHEMISTRY 107, 332–346 (1993)

Distribution and Ionic Diffusion Path of Silver in γ-Ag_8GeTe_6: A Temperature Dependent Anharmonic Single Crystal Structure Study

F. BOUCHER, M. EVAIN,* AND R. BREC

*I.M.N., Laboratoire de Chimie des Solides, 2 rue de la Houssinière, 44072 Nantes, Cedex 03, France

Received November 30, 1992; accepted February 24, 1993

The localization and diffusion of silver species in the high temperature allotropic form γ-Ag_8GeTe_6 (space group $F\bar{4}3m$, a = 1156.56(4)pm, Z = 4) is revisited from temperature dependent X-ray data with the aid of refinements including anharmonic thermal motions (Gram–Charlier expansion of the structure factor). γ-Ag_8GeTe_6 is built upon the stacking of $GeTe_4$ tetrahedral units and free tellurium atoms that manages five different tetrahedral sites available for silver ions. A coherent silver distribution over the voids is evidenced by testing three models corresponding to different tensor orders for the atomic displacement parameters (ADP). Three diffusion paths between the preponderant silver sites are revealed by means of joint probability density functions (jpdf) and it is shown through the temperature dependence of those jpdf that the silver disorder is of the positional type.

Introduction

Ag_8MX_6 compounds (M = Si, Ge, or Sn; X = S, Se, or Te) have been known for many years (*1–5*). These materials exhibit one or two phase transitions (*5*) attributed to the setting up of an ordering of the Ag^+ cations within the MX_6 matrix. On the one hand, powder studies have shown (*5*) that all high temperature allotropic forms (labeled γ-Ag_8MX_6) present the same network, fcc Bravais type and apparently the same space group. On the other hand, single crystal studies have shown (*6–9*) a lower symmetry for all low temperature allotropic varieties. This symmetry lowering upon transition is different from one compound to another. For instance, α''-Ag_8GeS_6 (*6*) and α''-Ag_8SiS_6 (*7*) crystallize in the $Pna2_1$ orthorhombic space group, β'-Ag_8GeSe_6 (*8*) adopts the $Pmn2_1$ space group, and α-Ag_8SiTe_6 (*9*) remains cubic but with the loss of the F centering and a doubling of the a parameter. The structure analyses of those low temperature phases reveal that the silver atoms are localized in low coordination sites (linear to tetrahedral). It seems that the silver arrangements are stabilized through the setting up of relatively short Ag–Ag distances (299 and 289 pm in β'-Ag_8GeSe_6 and α''-Ag_8SiS_6, respectively, and 293 pm in α''-Ag_8GeS_6), hinting at possible d^{10}–d^{10} homoatomic interactions (*10*). It is also observed that, in the high temperature forms, silver is highly disordered, reflecting ionic conducting properties for the phases (*11–13*).

Several years ago, three structural studies (*14–16*) were carried out on γ-Ag_8GeTe_6, which is stable at room temperature. In spite of the very important disorder introduced on the cationic subnetwork, none of them yielded coherent results, with, in particular, meaningful Ag–Te and Ag–Ge distances. Only recently, another structural determination performed on γ-Ag_8SiTe_6 (*9*) could deliver a satisfactory Ag^+ distribution and could evidence some diffusion paths for the cations. In particular, it was observed that

* To whom correspondence should be addressed.

0022-4596/93 $5.00

the silver cations moved within clusters build up from 24 tellurium tetrahedra. However, the ionic conductivity could not be fully explained since no intercluster pathways could be found.

To check, and eventually improve, the model found for γ-Ag_8SiTe_6 (in particular the apparent lack of intercluster diffusion paths), a temperature dependent anharmonic single crystal study was carried out on isotypic γ-Ag_8GeTe_6. The results of this study are reported in this article.

Experimental

Synthesis

Two different techniques have been used for the preparation of the γ-Ag_8GeTe_6 samples, one for powder studies (lattice parameter least squares refinements) and one for the single crystal X-ray structure determination.

For the former technique, the elements were taken in stoichiometric proportion and placed in a carbon tube, itself inclosed in an evacuated silica tube (this precaution being taken to avoid the formation of the Ag_8SiTe_6 silicon derivative through a reaction with silica). After a heating up of the mixture at 1073 K for a week, the sample was quenched in melting ice to prevent any peritectic decomposition (Gorochov showed (*5*) a noncongruent melting point at 918 K). Although the powder pattern did not reveal any crystallized impurity, a one week annealing was made. This extra step improved the sample crystallinity but also allowed the crystallization of an impurity that revealed itself through the emergence of a few weak peaks attributable to the hexagonal phase Ag_7Te_4 (*17*).

Since this technique did not supply any single crystal suitable for X-ray data recording, a transport method with iodine as the transport agent was attempted. Some Ag_8GeTe_6 powder and few I_2 crystals were placed in a furnace at 1073 K for 7 days and subsequently cooled down to room temperature within 8 days. Well shaped large single crystals were hence obtained.

Powder Diagram Study

The γ-Ag_8GeTe_6 X-ray powder pattern was obtained at room temperature on a Siemens D5000 diffractometer (Cu$K\alpha$1 radiation, incident beam Ge monochromator, scintillation detector). Data were collected with a 0.02° (2θ) step scan and a 50-sec counting time in the 10–110° (2θ) angular range. The diagram was analyzed with the PROLIX program (*18*). The a parameter was least squares refined from 34 reflections to a 2θ mean deviation of 0.0034° (Table I), yielding a value of a = 1156.56 (4) pm. It is in agreement with the cell parameters already published by Rysanek *et al.* (*14*) (a = 1156.6(2) pm) and Geller (*16*) (a = 1158(2) pm).

Single Crystal Study

The selected single crystal, cleaved from a large one to be small enough for the X-ray study, was glued at the tip of a quartz capillary with a "Torr Seal Vacuum Kit." The diffracted intensities were measured at two different temperatures (293 K and 400 K) on a CAD4 Enraf-Nonius diffractometer equipped with an AET hot gas (nitrogen) blowing apparatus. Mo$K\alpha$ radiation and a graphite monochromator were used. The detailed recording conditions are reported in Table II. To allow for semiempirical absorption corrections, psi measurements of the intensities of four $\chi \approx 90°$ reflexions were undertaken.

The usual corrections (i.e., absorption and Lorentz-polarization) were applied. Since a high temperature electronic diffraction study did not reveal any significant TDS (thermal diffusion scattering) effect, no corrections were applied. Diffracted intensities were averaged in agreement with the Laue symmetry of the noncentrosymmetric $F\bar{4}3m$ space group. This space group, already considered in previous studies on γ-Ag_8GeTe_6 (*14*, *16*) and on γ-Ag_8SiTe_6 (*9*), proved to be

TABLE I

γ-Ag_8GeTe_6 Room Temperature Indexed Powder Pattern

d_{obs} (pm)	d_{cal} (pm)	h k l	I_{rel}
667.5	667.7	1 1 1	4
409.0	408.9	2 2 0	4
348.75	348.72	3 1 1	39
333.95	333.87	2 2 2	100
265.36	265.33	3 3 1	14
236.08	236.08	4 2 2	37
222.55	222.58	3 3 3	93
204.44	204.45	4 4 0	35
195.505	195.494	5 3 1	18
192.740	192.760	4 4 2	24
182.863	182.868	6 2 0	6
176.368	176.374	5 3 3	14
174.357	174.358	6 2 2	13
161.953	161.951	5 5 1	8
154.544	154.552	6 4 2	2
150.574	150.571	5 5 3	11
144.558	144.570	8 0 0	17
141.292	141.296	7 3 3	1
136.313	136.302	8 2 2	4
133.551	133.548	5 5 5	9
132.661	132.666	6 6 2	11
129.295	129.307	8 4 0	2
126.955	126.949	7 5 3	10
123.280	123.290	6 6 4	3
121.239	121.240	9 3 1	5
118.041	118.041	8 4 4	10
116.245	116.239	7 5 5	2
113.408	113.410	8 6 2	2
111.808	111.809	7 7 3	4
111.288	111.290	6 6 6	7
107.852	107.850	9 5 3	1
104.287	104.283	7 7 5	2
101.048	101.049	9 5 5	4
97.748	97.747	10 6 2	5

the correct one. Finally, 325 and 300 independent reflections with $I>2.5\sigma(I)$ were left for the refinements at 293 K and 400 K with agreement factors on the intensity averaging of 5.5% and 5.2%.

To compare the structure of the γ-Ag_8GeTe_6 phase to that of the γ-Ag_8SiTe_6, previously published, the data of the latter one were reprocessed with the same reject criteria ($I>2.5\sigma$ (I)). Thus 329 independent reflections were obtained.

Structure Refinements

Refinements Description

All refinements were carried out with the PROMETHEUS program (*19*) that allows calculations with anharmonic atomic displacement parameters (ADPs) (*20*) such as the Gram–Charlier expansion of the structure factor (*21, 22*). The atomic scattering

TABLE II

Analytical and Crystallographic Data: Parameters of the X-Ray Data Collections

1. Physical, crystallographic, and analytical data		
Formula	Ag_8GeTe_6	
Space group	$F\bar{4}3m$ (No. 216)	
Room temperature crystallographic constants	a = 1156.56(4) pm, Z = 4	
Molecular weight	1701.1 g.mol^{-1}	
Density (calc.)	7.304	
Absorption factor	μ(Mo$K\alpha$) = 228.1 cm^{-1}	
Crystal size	<0.06 × 0.06 × 0.12 mm^3	
2. Data collection and reduction		
Radiation	Mo$K\alpha$	
Monochromator	oriented graphite (002)	
Scan mode	$\omega/2\theta$	
Scan angle	1.5 + 0.35 tan(θ)	
Recording range	2–35°	
Standard reflections	2 2 2, 1 −5 1, 4 −4 0 (every 3600 sec)	
Reflections for crystal matrix orientation	25	
Temperature	293 K	400 K
Recorded reflections in a ¼ space	1926	1960
Independant reflections with $I > 2.5\ \sigma(I)$	325	300
$R_I = \Sigma \lvert I - I_{avr} \rvert / \Sigma I$	5.5%	5.2%

factors and the anomalous dispersion correction values were taken from the International Tables for X-ray Crystallography (*21*). The atomic parameters, the scale factor, and the secondary isotropic extinction coefficient (*23*) were obtained through minimization of the $R_w = (\Sigma w(|F_0| - |F_c|)^2/\Sigma w F_0^2)^{1/2}$ function with $w = 1/\sigma(F_0)^2$.

The germanium and tellurium atomic positions were kept identical to those given in the previous structural description of γ-Ag_8GeTe_6 (*16*). Since none of the previous studies on this phase had given a correct silver distribution (see below), the silver atomic positions were taken from the results of the γ-Ag_8SiTe_6 phase study (*9*). However, to decrease the correlation coefficients, to facilitate the refinement convergence, and to better model the silver diffusion paths, an anharmonic development of the ADPs was used. The three following models have been compared in this study:

—a classical distribution model (split model), completely identical to that used in the γ-Ag_8SiTe_6 phase (9). Three partially occupied silver positions Ag1 (48*h*), Ag2 (48*h*), and Ag3 (96*i*) are refined with anisotropic ADPs. This model will be labeled model ***222*** since the anisotropic ADPs correspond to second order tensors.

—a first mixed model, i.e., intermediary between a purely anharmonic and a split model. This approach is known for ionic conductor compounds exhibiting a continuous distribution of mobile species (*24*). In this model, the preponderant Ag1 position is introduced with a third order tensor anharmonic ADP (*25*). The Ag2 position is considered with an anisotropic ADP whereas the minority Ag3 position is isotropically refined. This will be the ***321*** model.

—a second mixed model, ***322*** model, is obtained through the taking into account of a second order tensor for the ADP of Ag3, i.e., an anisotropic refinement for this atom.

Many other models were tested with, in particular, fourth order tensor anharmonic ADP for the Ag1 position. However, the use of even high order anharmonic tensors, describing kurtosis phenomena, proved less fruitful than odd coefficient developments modeling a skewness of the probability density function (*pdf*).

The three aforementioned models were tested on both the Ag_8GeTe_6 293 K and 400 K recording data and on the Ag_8SiTe_6 293 K reflection set for comparison's sake. It is noted that, for each model, constraints were set up on silver occupation ratios in order to keep 32 silver atoms per cell, in agreement with the title formula (letting the individual silver occupation ratio fluctuate independently did not lead to a significant departure from it).

Refinements Results

As a standard practice, the acceptability of a model was judged from the values of the agreement factors R, R_w, and S, from the number of variables versus the number of data (Hamilton tests (*26*)), and through the examination of Fourier difference maps. In addition, the shape of the joint probability density function (jpdf) (*19, 27*) was carefully observed since, in the case of an anharmonic model, it should not contain important negative regions to be meaningful (*24*). In Table III have been reported the reliability factors and the Hamilton test results (the Fourier differences maps that were almost the same from one model to the other are not presented). The jpdfs for the mixed models had all a physical meaning. All Ag1, Ag2, and Ag3 refined atomic parameters are given in Tables IVa, IVb, and IVc for the ***222***, ***321***, and ***322*** models, respectively. Since there was no change from one model to another concerning the germanium (or silicon) and tellurium atomic parameters, results are reported in Table V for the ***322*** model only.

TABLE III

RESULTS OF REFINEMENTS FOR EACH MODEL AND EACH TEMPERATURE DATA SET

1. Ag_8GeTe_6: Data Collection at 293 K

	Models		
	222	***321***	***322***
	Agreement factors		
R (%)[a]	3.81	3.66	3.55
R_w (%)[b]	4.11	3.97	3.87
S[c]	1.03	0.99	0.98
	Hamilton test		
Nb. param.	31	32	37
Nb. data	325	325	325
$\Re_{Ham}$	ref.	1.014	1.033
$\Re_{exp}$	ref.	1.035	1.062

2. Ag_8GeTe_6: Data Collection at 400 K

	Models		
	222	***321***	***322***
	Agreement factors		
R (%)[a]	5.49	5.42	5.07
R_w (%)[b]	5.35	5.30	5.11
S[c]	1.32	1.31	1.26
	Hamilton test		
Nb. param.	31	32	37
Nb. data	300	300	300
$\Re_{Ham}$	ref	1.015	1.036
$\Re_{exp}$	ref.	1.013	1.083

3. Ag_8SiTe_6: Data Collection at 293 K

	Models		
	222	***321***	***322***
	Agreement factors		
R (%)[a]	3.21	2.92	2.80
R_w (%)[b]	3.39	3.12	3.03
S[c]	1.13	1.04	1.02
	Hamilton test		
Nb. param.	31	32	37
Nb. data	329	329	329
$\Re_{Ham}$	ref.	1.014	1.032
$\Re_{exp}$	ref.	1.100	1.146

Note: Weighting scheme: $1/\sigma(F)^2$.

[a] Reliability factor: $R = \Sigma||F_0| - |F_c|| / \Sigma|F_0|$.

[b] Reliability factor: $R_w = [\Sigma_w(|F_0| - |F_c|)^2/\Sigma_w F_0^2]^{1/2}$.

[c] Goodness-of-fit (error in an observation of unit weight): $S = [\Sigma_w(|F_0| - |F_c|)^2/\text{degrees of freedom}]^{1/2}$.

As observed by Bachmann and Schulz (*24*), correlations between refined parameters decrease significantly when going from a classical split model to an anharmonic one. Indeed, the structure refinements using the anharmonic ***321*** and ***322*** models proved more stable than the classical calculation with the ***222*** model. In addition, the examination of the agreement factors and of the Hamilton tests (Table III) showed that model ***322*** yielded better results than model ***321***. Consequently, this model (***322***) was considered the more reliable and kept for the structural description of the phases.

Structural Results

Review

Since the first synthesis of γ-Ag_8GeTe_6 (*3*), three different structural studies were made from single crystal data (*14–16*). In each work, the difficulty encountered in solving the structure originated in the strong silver disorder, in relation with the ionic conduction behavior of the γ varieties (*11–13*).

In 1975, from data collected on films, Rysanek *et al.* (*14*) presented a first model with six partially occupied silver positions in a cubic cell (space group $F\bar{4}3m$). Because of a lack of observable reflections (169 independent *hkl*), the positions could only be refined with isotropic ADPs. The refinement led to a rather high reliability factor of 7.4%. Geller (*16*) showed later the inconsistency of the results, short Ag–Te distances being calculated (186 pm for Ag2–1–Te1 and 210 pm for Ag3–Te3).

Another distribution model was later put forward by von Unterrichter and Range (*15*). The recording performed on an automatic diffractometer revealed a pseudocubic cell with an $R3$ symmetry. In this study, 13 partially filled silver positions were refined with anisotropic ADPs, leading to an R factor of 6.0%. Here again, the observation of short interatomic distances revealed a doubtful silver distribution. In effect, a short Ge–Ag13 distance of 256 pm is calcu-

TABLE IV

Refined Parameters

Data	Ag_8GeTe_6 at 293 K			Ag_8GeTe_6 at 400 K			Ag_8SiTe_6 at 293 K		
Atom	Ag1	Ag2	Ag3	Ag1	Ag2	Ag3	Ag1	Ag2	Ag3
				a. Model ***222***					
τ	0.21(5)	0.22(6)	0.117	0.19(4)	0.22(3)	0.12	0.185(13)	0.246(11)	0.118
x	0.4272(12)	0.469(8)	0.365(4)	0.420(4)	0.461(4)	0.380(5)	0.4271(8)	0.463(2)	0.368(3)
y	0.427	0.469	0.434(2)	0.420	0.461	0.443(3)	0.427	0.463	0.4388(15)
z	0.2320(11)	0.219(3)	0.224(2)	0.244(4)	0.224(2)	0.214(4)	0.2232(10)	0.2275(10)	0.228(2)
B_{eq}	4.4(6)	7(3)	15(2)	12(2)	10(2)	14(2)	4.0(3)	13.7(11)	16.3(15)
U_{11}	0.052(4)	0.12(6)	0.18(3)	0.10(2)	0.16(3)	0.32(4)	0.059(4)	0.22(2)	0.30(3)
U_{22}	U_{11}	U_{11}	0.115(14)	U_{11}	U_{11}	0.060(11)	U_{11}	U_{11}	0.083(7)
U_{33}	0.062(13)	0.035(7)	0.28(3)	0.24(5)	0.037(7)	0.15(3)	0.035(4)	0.074(6)	0.24(2)
U_{12}	−0.019(11)	0.08(6)	−0.11(2)	0.05(2)	0.10(3)	−0.11(2)	−0.004(5)	0.19(2)	−0.120(12)
U_{13}	−0.004(3)	−0.03(2)	0.14(2)	−0.08(2)	−0.044(10)	0.12(3)	−0.004(3)	−0.109(10)	0.18(2)
U_{23}	U_{13}	U_{13}	−0.14(2)	U_{13}	U_{13}	−0.065(13)	U_{13}	U_{13}	−0.117(11)
				b. Model ***321***					
τ	0.32(2)	0.27(2)	0.038	0.34(4)	0.23(4)	0.051	0.34(2)	0.21(2)	0.057
x	0.4135(12)	0.462(2)	0.336(4)	0.415(2)	0.464(5)	0.347(3)	0.4184(10)	0.470(3)	0.3447(13)
y	0.414	0.462	0.461(3)	0.415	0.464	0.462(3)	0.418	0.470	0.4564(13)
z	0.2384(15)	0.2233(11)	0.197(3)	0.241(2)	0.221(2)	0.198(3)	0.2390(10)	0.221(2)	0.2060(11)
$B_{eq}(B_{iso})$	9.0(8)	11.4(14)	4.2(8)	8.7(9)	8(2)	4.3(8)	6.5(3)	8.2(14)	4.2(3)
U_{11}	0.108(9)	0.19(2)		0.097(8)	0.13(3)		0.079(3)	0.13(2)	
U_{22}	U_{11}	U_{11}		U_{11}	U_{11}		U_{11}	U_{11}	
U_{33}	0.129(11)	0.044(5)		0.14(2)	0.036(6)		0.090(6)	0.043(4)	
U_{12}	−0.021(9)	0.15(2)		0.000(10)	0.06(3)		0.006(4)	0.10(3)	
U_{13}	−0.027(4)	−0.066(10)		−0.031(6)	−0.032(9)		−0.026(2)	−0.045(10)	
U_{23}	U_{13}	U_{13}		U_{13}	U_{13}		U_{13}	U_{13}	
C_{111}	−0.23(5)			−0.17(4)			−0.11(2)		
C_{222}	C_{111}			C_{111}			C_{111}		
C_{333}	0.37(10)			0.26(9)			0.14(3)		
C_{112}	0.03(2)			0.01(2)			0.023(8)		
C_{122}	C_{112}			C_{112}			C_{112}		
C_{113}	0.01(3)			0.03(3)			0.032(9)		
C_{133}	−0.16(3)			−0.11(3)			−0.076(12)		
C_{223}	C_{113}			C_{113}			C_{113}		
C_{233}	C_{133}			C_{133}			C_{133}		
C_{123}	0.08(3)			0.06(3)			0.016(9)		
				c. Model ***322***					
τ	0.33(2)	0.25(2)	0.041	0.33(4)	0.20(4)	0.066	0.34(2)	0.19(2)	0.067
x	0.4145(12)	0.464(3)	0.335(4)	0.417(2)	0.470(6)	0.353(5)	0.4201(13)	0.474(3)	0.347(2)
y	0.415	0.464	0.457(3)	0.417	0.470	0.457(4)	0.420	0.474	0.454(2)
z	0.239(2)	0.2234(13)	0.199(3)	0.241(2)	0.221(2)	0.205(4)	0.2389(10)	0.220(2)	0.208(2)
B_{eq}	8.9(8)	11.6(15)	4.3(15)	8.7(9)	8(3)	6(2)	6.3(3)	7.7(15)	5.5(9)
U_{11}	0.104(10)	0.20(3)	0.06(2)	0.087(7)	0.13(5)	0.09(3)	0.074(3)	0.12(3)	0.09(2)
U_{22}	U_{11}	U_{11}	0.030(11)	U_{11}	U_{11}	0.036(15)	U_{11}	U_{11}	0.042(6)
U_{33}	0.131(11)	0.046(6)	0.07(2)	0.16(2)	0.038(7)	0.09(2)	0.091(6)	0.043(5)	0.074(10)
U_{12}	−0.020(9)	0.15(3)	−0.006(12)	0.014(8)	0.06(5)	−0.03(2)	0.011(4)	0.08(3)	−0.013(8)
U_{13}	−0.030(4)	−0.071(11)	−0.02(2)	−0.038(6)	−0.033(15)	−0.00(2)	−0.028(3)	−0.047(12)	0.005(11)
U_{23}	U_{13}	U_{13}	−0.026(11)	U_{13}	U_{13}	−0.044(15)	U_{13}	U_{13}	−0.020(7)
C_{111}	−0.19(6)			−0.11(4)			−0.07(2)		
C_{222}	C_{111}			C_{111}			C_{111}		
C_{333}	0.36(9)			0.21(9)			0.13(3)		
C_{112}	0.01(2)			−0.03(3)			0.009(8)		
C_{122}	C_{112}			C_{112}			C_{112}		
C_{113}	0.04(3)			0.08(3)			0.040(9)		
C_{133}	−0.16(3)			−0.15(4)			−0.081(11)		
C_{223}	C_{113}			C_{113}			C_{113}		
C_{233}	C_{133}			C_{133}			C_{133}		
C_{123}	0.08(3)			0.03(2)			0.016(9)		

Note. τ represents the occupation ratio of the position. Isotropic equivalent ADP defined as B_{eq} (10^4 pm^2) = $\frac{4}{3}\sum_i\sum_j \beta_{ij}a_ia_j$. The expression of the harmonic temperature factor is $\exp[-2\pi^2(U_{11}h^2a^{*2} + U_{22}k^2b^{*2} + U_{33}l^2c^{*2} + 2U_{12}hka^*b^* + 2U_{13}hla^*c^* + 2U_{23}klb^*c^*)]$ with U_{ij} in 10^4 pm^2. Third-order tensor elements C_{pqr} are multiplied by 10^4.

TABLE V

REFINED PARAMETERS OBTAINED WITH THE MODEL 3 2 2 FOR Ge (OR Si) AND TELLURIUM ATOMS FOR EACH DATA COLLECTION

Atom	Ge(Si)	Te1	Te2	Te3
	1. Ag_8GeTe_6: Data collection at 293 K[a]			
x	$\frac{3}{4}$	0.62269(10)	$\frac{1}{4}$	0
y	$\frac{3}{4}$	0.6227	$\frac{1}{4}$	0
z	$\frac{3}{4}$	0.6227	$\frac{1}{4}$	0
B_{eq}	1.12(5)	1.77(2)	5.35(13)	4.88(12)
U_{11}	0.0142(7)	0.0224(3)	0.068(2)	0.062(2)
U_{22}	U_{11}	U_{11}	U_{11}	U_{11}
U_{33}	U_{11}	U_{11}	U_{11}	U_{11}
U_{12}	0	−0.0051(2)	0	0
U_{13}	0	U_{12}	0	0
U_{23}	0	U_{12}	0	0
	2. Ag_8GeTe_6: Data collection at 400 K[b]			
x	$\frac{3}{4}$	0.6229(2)	$\frac{1}{4}$	0
y	$\frac{3}{4}$	0.623	$\frac{1}{4}$	0
z	$\frac{3}{4}$	0.623	$\frac{1}{4}$	0
B_{eq}	1.43(7)	2.36(4)	5.4(2)	4.6(2)
U_{11}	0.0181(9)	0.0299(5)	0.069(2)	0.059(2)
U_{22}	U_{11}	U_{11}	U_{11}	U_{11}
U_{33}	U_{11}	U_{11}	U_{11}	U_{11}
U_{12}	0	−0.0064(4)	0	0
U_{13}	0	U_{12}	0	0
U_{23}	0	U_{12}	0	0
	3. Ag_8SiTe_6: Data collection at 293 K[c]			
x	$\frac{3}{4}$	0.62515(8)	$\frac{1}{4}$	0
y	$\frac{3}{4}$	0.625	$\frac{1}{4}$	0
z	$\frac{3}{4}$	0.625	$\frac{1}{4}$	0
B_{eq}	0.79(8)	1.76(2)	5.55(9)	4.79(8)
U_{11}	0.0100(9)	0.0223(2)	0.0704(12)	0.0607(10)
U_{22}	U_{11}	U_{11}	U_{11}	U_{11}
U_{33}	U_{11}	U_{11}	U_{11}	U_{11}
U_{12}	0	−0.00446(12)	0	0
U_{13}	0	U_{12}	0	0
U_{23}	0	U_{12}	0	0

Note. See note below Table IV.
[a]Extinction coefficient. $G + 1.24(8) \times 10^{-5}$.
[b]Extinction coefficient. $G = 1.24(6) \times 10^{-5}$.
[c]Extinction coefficient. $G = 1.4(1) \times 10^{-5}$.

lated (about the same as the Ag–Te bonding one) and an Ag5–Te2 bond of 216 pm (much too short even for a linear arrangement which normally establishes around 278 pm (*28*)).

The last model was published by Geller (*16*). In this study, two distributions were proposed in a cubic symmetry cell (space group $F\bar{4}3m$). In the first one, a reliability factor of 9.7% was obtained with four silver sites and a refinement both of the occupation ratios and of the anisotropic ADPs. In the second proposition, considered as the best one by Geller, seven silver sites were used (six with an isotropic and one with an anisotropic ADPs). A confidence factor of 8.2% was obtained. In both studies, the Ag5 site, identical to the Ge one, exhibits too short Ag–Te distances of 247 pm, whereas the total amount of the ionic radii (according to Shannon (*28*)) for silver in such a site is 299 pm. In addition, this site is of type III (see below) and it will be shown later that it is very unfavorable as far as the diffusion process is concerned. It is clear that these last reported structural descriptions present a certain number of questionable features.

Structure Description

The structure was satisfactorily refined to an R of 3.5% for room temperature data with correct Ag–Te and Ag–Ge distances (see below the discussion of these distances from the so-called "modes" derived from the jpdf).

The unit cell of γ-Ag_8GeTe_6 contains four Ag_8GeTe_6 units ($Z = 4$). The germanium and tellurium arrangement is that of the Ag_8MX_6 family (M = Si, Ge, or Sn, X = S, Se, or Te) (*6–9*), of the isotypic phases Ag_7TaS_6 (*29*), and of Ag_9GaSe_6 (*30*), for instance.

The germanium atoms (4*d*: $\frac{3}{4}, \frac{3}{4}, \frac{3}{4}$) are tetrahedrally coordinated by Te1 atoms (16*e*: $x, x, x, x \approx 5/8$). Those $GeTe_4$ entities are linked to each other by Ag^+ cations. The other tellurium atoms, Te2 (4*c*: $\frac{1}{4}, \frac{1}{4}, \frac{1}{4}$) and Te3 (4*a*: 0, 0, 0), have no germanium neighbors and are only bonded to silver atoms. The mobile character of the silver cations affects the Te2 and Te3 anions which present high ADPs: The B_{eq} are equal to 5.35(13) and 4.88(12) $\times 10^4$ pm^2 at 293 K and 5.4(2) and 4.6(2) $\times 10^4$ pm^2 at 400 K, respectively. These tellurium atoms will be referred to as "free tellurium" as opposed to those strongly linked to germanium atoms and which will be called "tied tellurium." The structural arrangement of the $GeTe_6$ part of the structure is shown in Fig. 1.

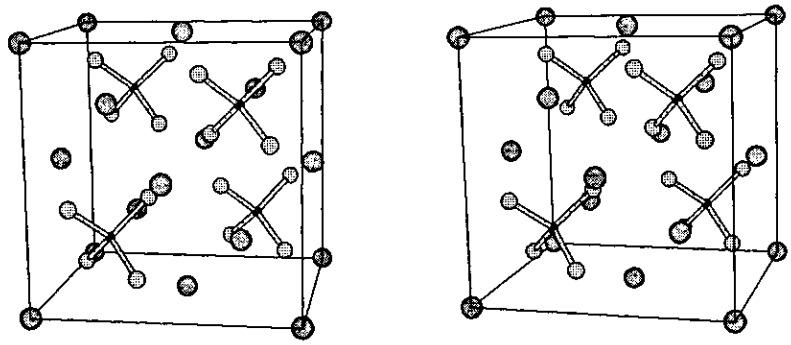

FIG. 1. Stereoscopic view of the $GeTe_6$ framework of γ-Ag_8GeTe_6. Large spheres correspond to tellurium atoms Te2 and Te3, medium spheres to tellurium atoms Te1, and small spheres to germanium atoms.

The $GeTe_6$ skeleton leaves numerous tetrahedral sites available for the silver distribution. In all, 132 such sites are found, belonging to the five different types listed in Table VI. These sites are characterized by the tellurium atoms that make them, the mean distance between the center of the site and the surrounding tellurium atoms, and, more important, the distance between this center of the site and the closest germanium atoms. Indeed, it has been shown in γ-Ag_8SiTe_6 (*9*) that three conditions were necessary for a site to be occupied. Firstly, for electrostatic repulsions reasons, the Ag^+ cation must be far enough from the germanium atom. Secondly, to accommodate a silver atom, the tetrahedral site must be large enough (it is to be recalled that, according to the ionic radii of Shannon (*28*), the Ag–Te distance in such an environment is 299 pm and 278 pm for a linear coordination). Thirdly, since a diffusion implies that the host sites be favorable for the cationic jumps, it must be easily distorted. For instance, a site made up from four Te1 atoms (belonging to rigid $GeTe_4$ entities) and containing no "free tellurium" is less able to distort itself than a site with three Te1 atoms and one "free tellurium" (Te2 or Te3), itself more rigid than a site with two "free tellurium."

TABLE VI

SILVER TETRAHEDRAL SITE OCCUPANCY PROBABILITY VERSUS SITE CHARACTERISTICS

Site	I	II	III	IV	V
Nbr of sites	48	16	4	48	16
Nbr of "tied Te"[a]	2	3	4	2	3
Nbr of "free Te"[b]	2	1	0	2	1
$d_{c\text{-}Ge}$ (pm)[c]	310	190	500	420	470
$\langle d_{c\text{-}Te}\rangle$ (pm)[d]	290	270	250	290	270
Occupancy probability[e]	high	very low	very low	very high	low

[a]Number of tellurium atoms of type Te1 of each site. These atoms are linked to germanium atoms.

[b]Number of tellurium atoms of type Te2 and Te3 of each site. These atoms are only linked to silver atoms and present large ADPs.

[c]$d_{c\text{-}Ge}$: Distances between the centers of the tetrahedral sites and germanium first neighbors.

[d]$\langle d_{c\text{-}Te}\rangle$: These means distances between the centers of the sites and tellurium atoms that make them characterize the site sizes.

[e]A tetrahedral sites presents a high filling probability if it is not too rigid, too small and if it is sufficiently away from germanium atoms.

From Table VI, one can see that the sites II and III are very unfavorable. In effect, the sites II are too close to the $GeTe_4$ tetrahedra and the sites III are too small and too "rigid." On the other hand, the sites of type IV, which number 48 per cell, are the most favorable and are largely implied in the diffusion process. Preponderantly filled Ag1

positions, refined with third order anharmonic ADPs, are located in the IV sites. An examination of the tetrahedral arrangement in the cell reveals that a tetrahedral site IV has common faces with another site IV, with two sites I (considered acceptable for the diffusion), and with a "rigid" site V. Consequently, the easiest jump from one site IV to the other seems to be through a common face. This type of jump was evidenced by means of the Ag2 positions and it was labeled direct jump, in agreement with the results on γ-Ag_8SiTe_6 (*9*). The jpdf maps (Fig. 2) show these types of jump present for each recording. Another diffusion path had also been shown for the γ-Ag_8SiTe_6 phase and had been called indirect jump. It corresponds to the jump from a site IV to another through site I. This jump, in which the Ag3 positions are implied, is, however, less populated than the previous one (Fig. 3). To summarize, silver ion was shown to diffuse within clusters formed by 12 tetrahedra of the types IV and 12 tetrahedra of the types I, such clusters containing 8 silver atoms. No intercluster pathway could be seen, the ionic conducting property of the phase remaining then unexplained.

The use of an anharmonic model for γ-Ag_8GeTe_6 structural description provides evidence for such an intercluster pathway already at room temperature. In Photograph 1, obtained at 293 K and corresponding to a cluster surface isodensity probability for the silver atoms, the third jump type is revealed by the distortion of the surface towards the site V. The pathway between clusters can be also observed in Photograph 2 that shows the same type of surface for three clusters partially represented around a tetrahedron of type V. These sites, previously considered as quite unfavorable for the diffusion (although not being the more unsuitable ones), seem, however, to allow for the diffusion of the Ag^+ cations between clusters.

The jpdf maps (Fig. 4) show that this jump observed at 293 K in Ag_8GeTe_6 is also observed at higher temperature with a higher filling ratio at the saddle point: 1.1% of the maximum of the tetrahedral site as opposed to 0.75% at 293 K. It is important to notice that no other diffusion path appeared at higher temperature and that the hypothesis put forward in the course of the study of Ag_8SiTe_6 (i.e., intercluster diffusion through

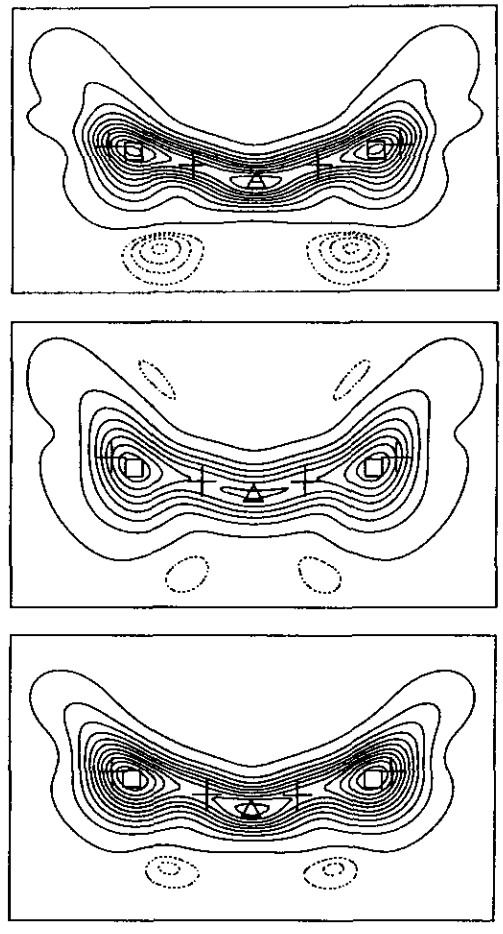

FIG. 2. Joint probability density function (jpdf) of silver along the direct jump path between two face sharing type IV tetrahedra for Ag_8GeTe_6 (293 K) at the top, Ag_8GeTe_6 (400 K) in the middle, and Ag_8SiTe_6 (293 K) at the bottom. The crosses denote the refined atom positions (means). The two middle crosses correspond to Ag2 positions and the two others to Ag1 positions. The squares and the triangle represent the Ag1* and Ag2* local maxima (modes) respectively. Contour lines are from 50×10^{-6} pm^{-3} to 2050×10^{-6} pm^{-3} in intervals of 200×10^{-6} pm^{-3} for positive probability (solid lines) and at -40, -30, -20 and -10×10^{-6} pm^{-3} for negative probability (dashed lines).

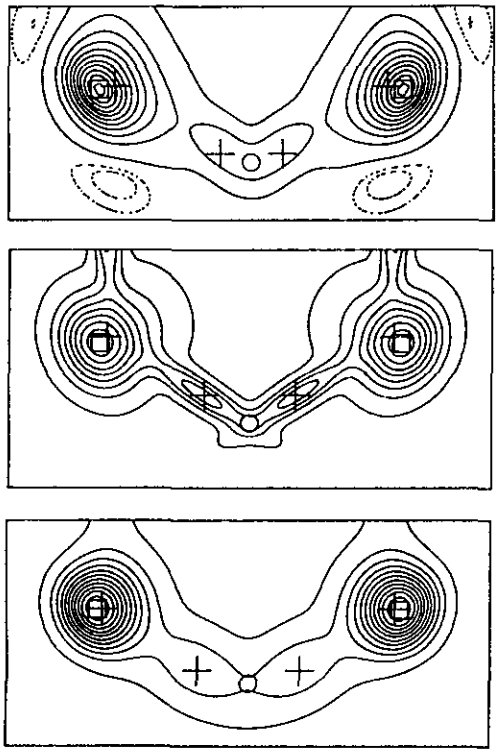

FIG. 3. Joint probability density function (jpdf) of silver along the indirect jump path between two edge sharing type IV tetrahedra through a type I tetrahedron for Ag_8GeTe_6 (293 K) at the top, Ag_8GeTe_6 (400 K) in the middle, and Ag_8SiTe_6 (293 K) at the bottom. The crosses denote the refined atom positions (means). The two middle crosses correspond to Ag3 positions and the two others to Ag1 positions. The squares and the circle represent the Ag1* and Ag3* local maxima (modes) respectively. Contour lines are from 50×10^{-6} to 2050×10^{-6} pm^{-3} in intervals of 200×10^{-6} pm^{-3} for positive probability (solid lines) and at -20 and -10×10^{-6} pm^{-3} for negative probability (dashed lines).

a type I tetrahedron) is thus not verified. The very weak filling of the "through type V" pathway calculated in Ag_8SiTe_6 (0.07% of the maximum of the tetrahedral site) may explain why it could not be detected in the course of this study.

Discussion

Validity of the Model

When an anharmonic model is used or when two pdfs overlap, it is necessary to argue about the probability density local maxima (called modes in distributions) to interpret the interatomic distances (*31*). Such mode positions obtained from jpdf maps have been reported in Table VII. They are labeled with an asterisk to differentiate them from the refined positions themselves.

The positions Ag1* and Ag2*, observed in the direct jump (Fig. 2), correspond to the centers of the type IV tetrahedra and of the triangular site common to two type IV tetrahedra, respectively. Considering the absence of a marked local maximum in the indirect jump (Fig. 3), the Ag3* position has been chosen at the center of the tetrahedron type I, within the mirror plane. In Table VIII are reported the Ag*–Te and Ag*–Ge distances, calculated for Ag_8GeTe_6 at room temperature. One can immediately see that the Ag*–Ge distances (425, 412, and 346 pm for Ag1*, Ag2*, and Ag3*, respectively) are large enough to exclude any interaction between these ions, which was expected but not observed with one of the previous models. The distances and angles, calculated for the tetrahedral sites Ag1*Te_4 and Ag3*Te_4 show that these sites are relatively distorted. One also observes that the mean Ag*–Te distance is slightly smaller than the ones calculated from the ionic radii (28); i.e., d_{mean}(Ag1*–Te) = 289 pm, d_{mean}(Ag3*–Te) = 292 pm, and $r(Ag^{2+}) + r(Te^{2-})$ = 299 pm. Likewise, the distorted triangular site Ag2*Te_3 presents a mean Ag*–Te distance smaller than expected for a cation in a linear environment (267 pm versus 278 pm). This decrease had already been discussed in the course of the study γ-Ag_8SiTe_6 and attributed to the fact that these sites were not fully occupied. In effect, because of the Ag^+ diffusion, these sites must be sometimes empty (small size sites) sometimes filled (sites with a size in agreement with proper Ag–Te distances). Consequently, in addition to important ADP values, one observes a size intermediary between an empty and filled site.

It is noted that our silver distribution model in γ-Ag_8MTe_6 phases (M = Si or Ge),

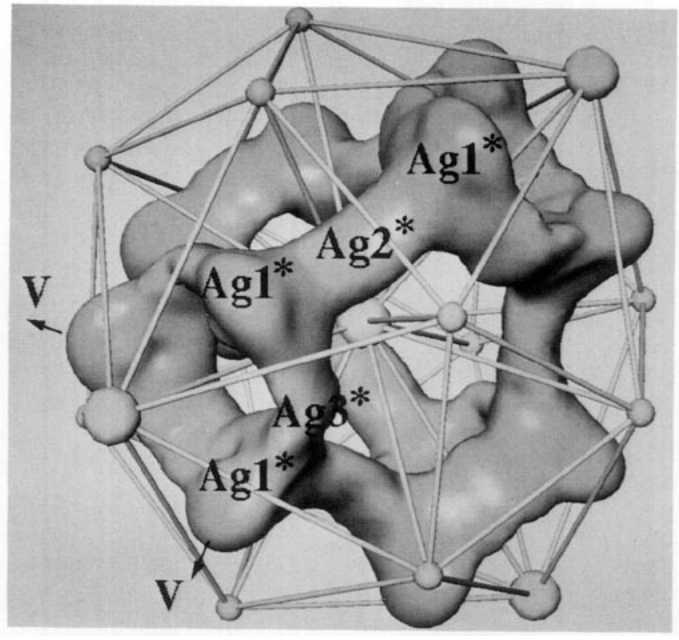

PHOTOGRAPH 1: Silver probability density surface of 20×10^{-6} pm^{-3} of a cluster for Ag_8GeTe_6 at 293 K. These clusters correspond to a distribution of 8 silver atoms over 24 tetrahedra of two different types. The large size spheres represent "free tellurium" atoms (Te2 or Te3) and the smaller ones represent the "tied tellurium" atoms (Te1) engaged in $GeTe_4$ groups. The direct jumps can easily be seen: from a type IV tetrahedron (Ag1* site) to another through the triangular face (Ag2* site). The indirect jumps correspond to jumps from type IV tetrahedron to another through a type I tetrahedron (Ag3* site). The distortion of the surface towards a type V tetrahedron hints at interclusters pathways (see Photograph 2).

unlike the previously published models, does not present any structural incompatibility. In addition, it has the advantage of allowing for an explanation of the ionic distribution in these phases. Let us underline the great resemblance existing between both room temperature Ag_8SiTe_6 and Ag_8GeTe_6 jpdf maps (i.e., a few dozen degrees above the transition). This observation suggests that such a model may be applied to other allotropic γ varieties of the Ag_8MX_6 type.

However, it is noticed that there exists another possible distribution of the atoms within the cell. In effect, the positions of the cation M^{4+} and anions Te^{2-} can undergo a translation of $\frac{1}{4}, \frac{1}{4}, \frac{1}{4}$, without modifying the results of the refinement. The M^{4+} cations occupy then the origin of the cell, the Te1 ions the x, x, x positions ($x \approx \frac{7}{8}$), the Te2 ions the $\frac{1}{2}, \frac{1}{2}, \frac{1}{2}$ and Te3 the $\frac{1}{4}, \frac{1}{4}, \frac{1}{4}$ ones. This impossibility to discriminate these two descriptions has been encountered on both the germanium and silicon derivatives.

Temperature Study of the Silver Distribution

To evidence the intercluster silver jumping pathway in γ-Ag_8SiTe_6, a higher temperature study was suggested (*9*). Since the diffusion mechanism was already evidenced with the room temperature experiment, there was then no point to further develop it. However, Bachmann and Schulz (*24*) have shown that an X-ray diffraction temperature study could discriminate the type of disorder present in the structure if one follows the change of the effective one-particle potential (opp) versus temperature (*32*). Such a study was initiated on Ag_8GeTe_6.

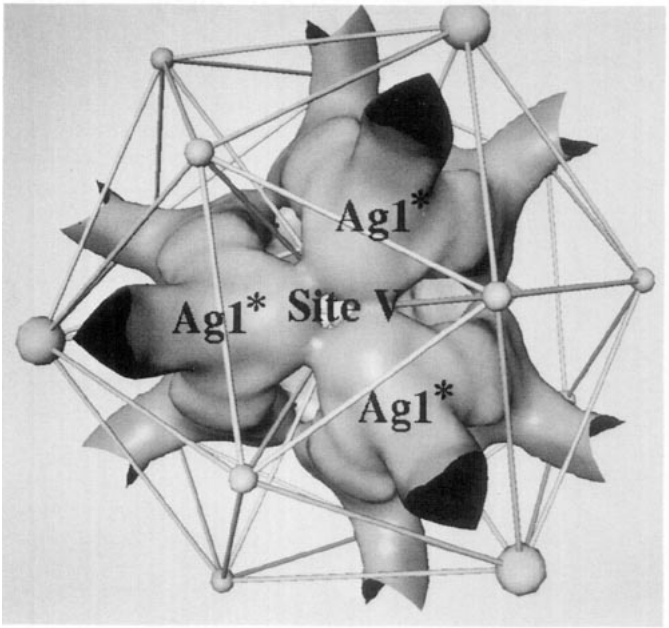

PHOTOGRAPH 2: Silver probability density surface of 12×10^{-6} pm^{-3} around a type V tetrahedron that shares 3 faces with 3 type IV tetrahedra (Ag1* site) of different clusters for Ag_8GeTe_6 at 293 K. Large and small size sphere represent the same as in Photograph 1. The inteclusters jump correspond to a pathway from site IV (Ag1* site) to another through a type V tetrahedron. Each tetrahedron of that type insures a silver diffusion between 3 different clusters.

The effective opp of Ag^+ was calculated along each pathway (direct, indirect and intercluster) for the two Ag_8GeTe_6 recordings (293 and 400 K) and for the Ag_8SiTe_6 room temperature one by using the following formula

$$V(\mathbf{r}) = V_0 - KT \ln [\text{jpdf}(\mathbf{r})],$$

where K is the Boltzmann constant, T the absolute temperature, jpdf (**r**) the joint probability density at the point corresponding to the vector **r**, and V_0 is the chosen potential of the normalization. jpdf(**r**) values have been normalized against the probability densities of the Ag1* sites: $V_0 = KT \ln [\text{jpdf}(\text{Ag1*})]$ (this formula is valid in the classical regime (i.e., above the Debye temperature) when it is supposed that the filling of the harmonic oscillator energy levels is controlled by the Boltzmann statistic).

In Fig. 5, the various diffusion pathways are labeled according to their density modes Ag1*, Ag2*, and Ag3*, i.e., Ag1*–Ag2*–Ag1* for the direct jump and Ag1*–Ag3*–Ag1* for the indirect one. Since one does not observe any density mode for the intercluster through type V jumps, one "V" was used to label this jump. The difference population of each jump leads to potential barriers of different height. The plot obtained for Ag_8GeTe_6 shows a dependence of the potential versus temperature. This is the characteristic of a crystal structure exhibiting a positional type disorder (*24*). Indeed, in disordered structures, i.e., in those showing positional disorders, the microscopic content of a given cell differs from the others. This is the case for the γ-Ag_8MTe_6 (M = Si and Ge) phases where the silver sites are partially occupied. Diffraction measurements give then information on the mean content of the cell and the pdf obtained represents the mean pdfs of all cells. Because of this space averaging, the obtained potential represents a pseudopotential which is wider than the true one

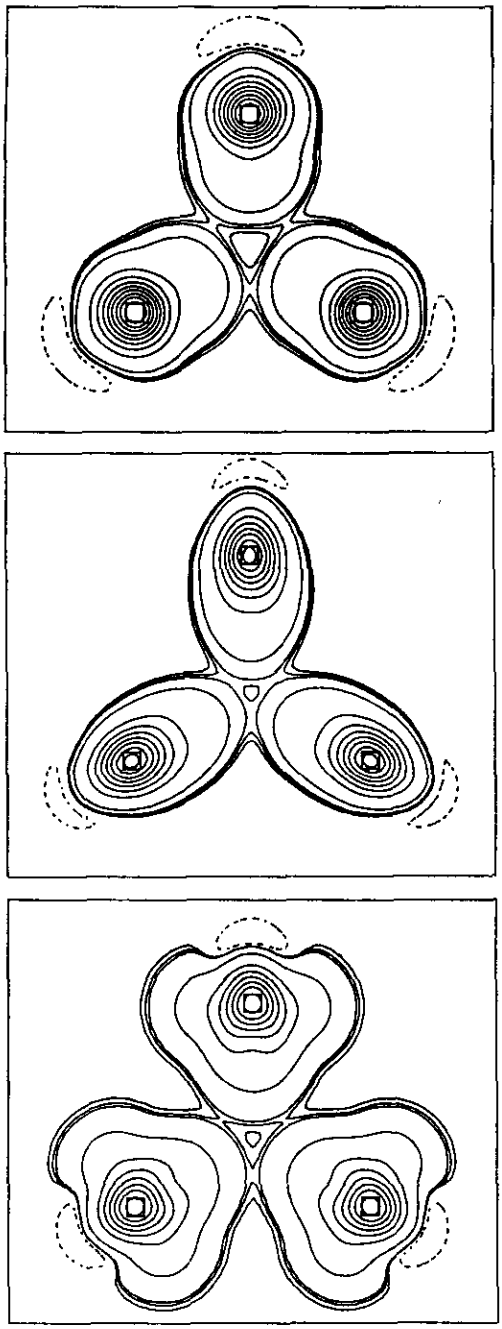

FIG. 4. Joint probability density function (jpdf) of silver along the interclusters jump path between three type IV tetrahedra through a type V tetrahedron for Ag_8GeTe_6 (293 K) at the top, Ag_8GeTe_6 (400 K) in the middle, and Ag_8SiTe_6 (293 K) at the bottom. The crosses denote the projection of refined atom positions (means) Ag1 and the squares represent the projection of Ag1* local maxima (modes). Positive probability contour lines (solid lines) are at 12, 16, 20, 50, 250, 450, . . . , 1650×10^{-6} pm^{-3} for Ag_8GeTe_6 and at 1, 2, 3, 50, 250, 450, . . . , 1250×10^{-6} pm^{-3} for Ag_8SiTe_6 and negative probability one (dashed lines) at -10×10^{-6} pm^{-3}.

and which changes with temperature. On the contrary, in positionally ordered but vibrationally disordered structures (such as ionic conductor Li_3N (*33*)) the anharmonic character observed for the ADPs is only

TABLE VII

ESTIMATED SILVER LOCAL MAXIMA (MODES)

Atom	x	y	z
1. Ag_8GeTe_6: Data collection at 293 K			
Ag1*	0.429	0.429	0.235
Ag2*	½	½	0.208
Ag3*	0.320	0.468	0.180
2. Ag_8GeTe_6: Data collection at 400 K			
Ag1*	0.429	0.429	0.234
Ag2*	½	½	0.211
Ag3*	0.324	0.479	0.176
3. Ag_8SiTe_6: Data collection at 293 K			
Ag1*	0.431	0.431	0.233
Ag2*	½	½	0.208
Ag3*	0.317	0.465	0.183

TABLE VIII

MAIN INTERATOMIC DISTANCES (pm) AND ANGLES (°) BASED UPON THE LOCAL MAXIMA OF THE jpdf (MODES) IN γ-Ag_8GeTe_6 AT 293 K

Ge–Te1	255.0(2) (×4)		
Ag1*–Ge	425		
Ag2*–Ge	412		
Ag3*–Ge	346		
Ag1*–Te1	284 (×2)	Te1–Ag1*–Te1	89.8
Ag1*–Te2	293	Te1–Ag1*–Te2	111.9 (×2)
Ag1*–Te3	296	Te1–Ag1*–Te3	111.8 (×2)
	$(Ag1^*–Te)_{avr}$289	Te2–Ag1*–Te3	116.5
Ag2*–Te1	280 (×2)	Te1–Ag2*–Te1	91.4
Ag2*–Te3	241	Te1–Ag2*–Te3	134.3 (×2)
	$(Ag2^*–Te)_{avr}$267		
Ag3*–Te1	297 (×2)	Te1–Ag3*–Te1	88.9
Ag3*–Te2	277	Te1–Ag3*–Te2	112.9 (×2)
Ag3*–Te3	297	Te1–Ag3*–Te3	107.9 (×2)
	$(Ag3^*–Te)_{avr}$292	Te2–Ag3*–Te3	121.6

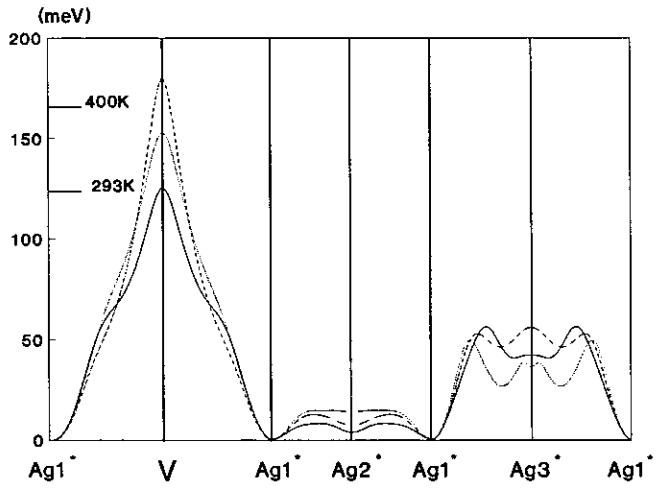

FIG. 5. Effective one-particle potential (opp) of Ag^+ along each jump for the three measurements. The direct jump from one Ag1* mode to another arises through the mode Ag2*, the indirect one through Ag3* and the intercluster one through a "V" (as type V tetrahedron). Solid lines correspond to Ag_8GeTe_6 at 293 K, dotted lines to Ag_8GeTe_6 at 400 K and dashed lines to Ag_8SiTe_6 at 293 K. In addition, the occupation probability 0.01 calculated from the Bose–Einstein distribution is shown at the two temperatures by the horizontal strokes.

linked to the thermal anharmonic vibrations. In that case, the potential energy calculated from the jpdf shows very little temperature dependence, it is characteristic of an effective opp. This means that it does represent the mean potential energy of an atom in interaction with all the others within the crystal. This opp can then be used to determine the activation energy of the ionic conductivity.

The jump that limits the ionic diffusion in the Ag_8MTe_6 phases is the intercluster one (see Fig. 5). Consequently, the height of the associated potential barrier could be compared to the energy activation of the ionic conductivity. However, since this type of phases shows positional disorder (the potential energy varies with temperature), it is then not reasonable to extract activation energies from the elastic diffraction data, the obtained potential being only a pseudoone.

Concluding Remarks

With an anharmonic description of the structure, we were able to solve the problem of the localization and diffusion of the Ag^+ ions in the Ag_8MTe_6 compounds. The structural study of Ag_8GeTe_6, combined with that of Ag_8SiTe_6, allowed to elucidate the intercluster diffusion phenomenon. Clearly, such a problem can only be tackled by using powerful refinement models.

To complete this work, it would be of interest to see if the diffusion model is the same in isotypical phases such as γ-Ag_8SiS_6 (stable above 507 K) or γ-Ag_8SiSe_6 (stable above 313 K) or even in compounds with higher or lower silver content such as Ag_9GaSe_6 and Ag_7TaS_6, respectively. In addition in these latter compounds, the role of the tetrahedral gallium and tantalum, rather electropositive species, could be evaluated.

References

1. H. HAHN, H. SCHULZE, AND L. SECHSER, *Naturwissenschaften* **52,** 451 (1965).
2. O. GOROCHOV, R. FICHET, AND J. FLAHAUT, *C. R. Acad. Sci. (Paris) Ser. C* **263,** 1422 (1966).
3. O. GOROCHOV AND J. FLAHAUT, *C. R. Acad. Sci. (Paris) Ser. C* **264,** 2153 (1967).
4. O. GOROCHOV, *C. R. Acad. Sci. (Paris) Ser. C.* **266,** 1059 (1968).
5. O. GOROCHOV, *Bull. Soc. Chim. Fr.* **6,** 2263 (1968).

6. G. EULENBERGER, *Monatsh. Chem.* **108,** 901 (1977).
7. B. KREBS AND J. MANDT, *Z. Naturfosch. B* **32,** 373 (1977).
8. D. CARRÉ, R. OLLITRAULT-FICHET, AND J. FLAHAUT, *Acta Crystallogr. Sect. B* **36,** 245 (1980).
9. F. BOUCHER, M. EVAIN, AND R. BREC, *J. Solid State Chem.* **100,** 341 (1992).
10. M. JANSEN, *Agnew. Chem. Int. Ed. Engl.* **26,** 1098 (1987).
11. I. S. OSIPISHIN AND B. I. GASII, *Visn. L'viv. Politekh. Inst.* **142,** 93 (1980).
12. I. S. OSIPISHIN AND B. I. GASII, *Fiz. Elektron (Lvov)* **27,** 37 (1982).
13. I. S. OSIPISHIN AND B. I. GASII, *Vestn. L'vov. Politekh. Inst.* **226,** 133 (1988).
14. N. RYSANEK, P. LARUELLE, AND A. KATTY, *Acta Crystallogr. Sect. B* **32,** 692 (1976).
15. J. VON UNTERRICHTER AND K. J. RANGE, *Z. Naturforsch. B* **33,** 866 (1978).
16. S. GELLER, *Z. Kristallogr.* **149,** 31 (1979).
17. THOMPSON AND BERRY, *Mem. Geol. Soc. Am.* 502 (1962).
18. P. DENIARD, M. EVAIN, J. M. BARBET, AND R. BREC, *in* "Materials Science Forum: EPDIC 1: European Powder Diffraction," R. Delhez and E. J. Mittemeijer, Eds., Vols. 79–82, pp. 365, Trans. Tech. Publications, Switzerland 1991; M. EVAIN, P. DENIARD, A. JOUANNEAUX, AND R. BREC, submitted.
19. U. H. ZUCKER, E. PERENTHALER, W. F. KUHS, R. BACHMANN, AND H. SCHULZ, *J. Appl. Crystallogr.* **16,** 358 (1983).
20. The expression Atomic Displacement Parameter (ADP) is used instead of Atomic Thermal Parameter because it includes either a dynamic disorder due to thermal vibrations or a positional disorder (static distribution) including static departure from the crystal symmetry. W. F. KUHS, *Acta Crystallogr. Sect. A* **48,** 80 (1992).
21. C. K. JOHNSON AND H. A. LEVY, *"International Tables for X-ray Crystallography,"* Vol. IV, Sect. 5, Kynoch Press, Birmingham (1974).
22. U. H. ZUCKER AND H. SCHULZ, *Acta Crystallogr. Sect. A* **38,** 563 (1982).
23. W. H. ZACHARIASEN, *Acta. Crystallogr.* **23,** 558 (1967).
24. R. BACHMANN AND H. SCHULZ, *Acta Cryst., A* **40,** 668 (1984).
25. The ADP obtained by the Gram–Charlier expansion for an atom k is given by: $T_k(\mathbf{H}) = T_k(\mathbf{H})_{\text{har}}[1 + ((2\pi i)^3/3!)\, C_k^{qr} h_p h_q h_r]$, where $T_k(\mathbf{H})_{\text{har}}$ is the harmonic part of the ADP of the atom k with $T_k(\mathbf{H})_{\text{har}} = \exp(-\mathbf{H}^T \beta_k \mathbf{H})$; C_k^{qr} are the refined anharmonic coefficients; and the variables h are the components of the reciprocal vector $\mathbf{H}$ obtained by applying the Einstein conventions summations.
26. W. C. HAMILTON, *Acta Crystallogr.* **18,** 502 (1965).
27. When several pdf's overlap (atomic positions too close), it is necessary to use the notion of joint probability density function (jpdf) to take this overlap into account. The jpdf of an atom type k at the position $\mathbf{r}$ is given by: $\text{jpdf}_k(\mathbf{r}) = \Sigma_i \omega_{ik} \text{pdf}_{ik}(\mathbf{r})$, where ω_{ik} is the occupancy of position i by an atom of type k and the sum is taken over all positions that can be occupied by the atom of type k.
28. R. D. SHANNON, *in* "Structure and Bonding in Crystals" (M. O'Keeffe and A. Navrotsky, Eds.), Vol. 2, p. 61, Academic Press, San Diego (1981).
29. H. WADA AND M. ONODA, *J. Less-Common Metals,* **175,** 209 (1991).
30. J. P. DELOUME, R. FAURE, AND H. LOISELEUR, *Acta Crystallogr. Sect. B* **34,** 3189 (1978).
31. The "mean" is simply the first-order term in the series expansion (i.e., the refined atom position) and the "mode" is given by a local maximum in the pdf. W. H. KUHS, *Acta Cryst., A* **39,** 148 (1983).
32. The effective one-particle potential is the average potential energy of an atom caused by the interactions with all other atoms of the crystal. In the classical limit one obtains the ADP of an atom k as a mean over all displacements $\mathbf{u}_k$ of this atom in the potential V_k, each displacement weighed by its thermodynamic probability: $T_k(\mathbf{H}) = \int \exp(-V_k/KT) \exp(2\pi i\, \mathbf{H} \cdot \mathbf{u}_k) d^3\mathbf{u} / \int \exp(-V_k/KT)\, d^3\mathbf{u}$ where K is the Boltzmann constant and T the absolute temperature.
33. U. H. ZUCKER AND H. SCHULZ, *Acta. Crystallogr. Sect. A* **38,** 568 (1982).